Canadian Chemical Transactions Year 2016 | Volume 4 | Issue 3 | Page 362-388

Research Article

DOI:10.13179/canchemtrans.2016.04.03.0306

Synthesis, Spectroscopic Investigation and Computational study of 4–((4–fluorophenyl)diazenyl)–2–formylphenyl methyl carbonate

A. Arokiasamy[a], G. Manikandan[b*], V. Thanikachalam[a], and K. Gokula Krishnan[a]

[a]*Department of Chemistry, Annamalai University, Annamalai Nagar–608 002, Tamil Nadu, India.*
[b]*Chemistry Section (FEAT), Annamalai University, Annamalai Nagar–608 002, Tamil Nadu, India.*

**Corresponding Author, Email: phdmani@gmail.com Mobile: +91-9994325507*

Received: *April 24, 2016* ***Revised:*** *July 1, 2016* ***Accepted:*** *July 16, 2016* ***Published:*** *July 28, 2016*

Abstract: 4–((4–fluorophenyl)diazenyl)–2–formylphenyl methyl carbonate (FFPMC) has been synthesized from 5–((4–fluorophenyl)diazenyl)–2–hydroxybenzaldehyde (FPDB) and methyl chloroformate. Theoretical studies such as polarizability, first order hyperpolarizability, zero–point vibrational energy and natural bonding orbital (NBO) analysis were carried out for the title compound using Hatree–Fock (HF) and Density Functional Theory (DFT) methods with 6–31+G(d,p) basis set. Also, the molecular structure, vibrational frequencies, dipole moment and molecular electrostatic potential energies have been calculated. The comparison in between the experimental and the theoretical values of FT-IR, FT-Raman vibrational spectra and NMR (^{1}H and ^{13}C) have also been discussed.

Keywords: Methyl carbonate, Hyperpolarizability, DFT, HOMO–LUMO, NBO.

1. INTRODUCTION

In our day to life, azobenzene derivatives play a vital role along with rapidly increasing applications in both industry and scientific laboratories [1–7] (e.g., solvents and synthetic blocks). Similarly, organic carbonates [8–11] being versatile compounds are used as solvents or reagents in the chemical industry as electrolytes in lithium batteries and as fuel additives [12]. They are also frequently used in biological/medicinal fields [13], agrochemicals [14], pharmaceuticals [15] and synthetic intermediates [16]. Nowadays, the substituted chloroformates reagents [17–19] are used for preparation of organic carbonates as they are easy to handle nontoxic in nature as well as have good reactivity. Hence, methyl chloroformate is useful in the synthesis of azo organic carbonates. Literature survey reveals that DFT calculations and experimental studies on FFPMC compound have not been reported so far. Therefore, the present work deals with the synthesis of FFPMC, experimental and theoretical investigations such as FT–IR, FT–Raman, NMR, HOMO–LUMO and NBO analysis of FFPMC by HF and DFT (B3LYP) methods with 6–31+G(d,p) as basis set.

2. EXPERIMENTAL

2.1 Synthesis of FFPMC

In the present work, two steps were adopted for the synthesis of FFPMC. The first step involved in the synthesis of FPDB by the diazotization of 4–fluroaniline (1 eq) was carried out with $NaNO_2$ in the presence of Conc. HCl at 0–5ºC, then to the diazotised mixture, salicylaldehyde (1 eq) was added drop wise [20]. After 3-4 h stirring, 80% of FPDB was formed. In the second step, a reaction mixture containing a solution of FPDB (0.62 g), dichloromethane (5 mL) and potassium carbonate (0.54 g, 4.25 mmol) were stirred 15 min, then methyl chloroformate (0.3 mL, 3.75 mmol) was added drop wise to the reaction mixture during a period of 15 min. This reaction mixture was stirred at 28–30 ºC for 6 h and the progress of the reaction was monitored by thin layer chromatography. After completion of the reaction, the reaction mixture was diluted with water (20 mL) and extracted with dichloromethane (2×20 mL). The combined organic layer was washed with water (2×20 mL) and brine solution (20 mL) and dried over anhydrous sodium sulphate (2.5 g), filtered and concentrated under reduced pressure. The crude product was then recrystallised from ethanol to get 70% of the purified FFPMC [19]. The synthetic route of FFPMC is outlined in Scheme 1.

2.2 Spectral measurements

The melting point was measured in open capillary and is uncorrected. FT–IR spectrum was recorded on Thermo Nicolet iS5 FT–IR spectrometer in the range of 400 to 4000 cm^{-1} by ATR in room temperature with number of scans equals 16 at Annamalai University, Annamalai Nagar, India. FT–Raman spectrum was recorded on Bruker: RFS 27 spectrometer. The spectral measurements were carried out at SAIF, Indian Institute of Technology, Chennai, India. The spectral features are reported in wavenumber (cm^{-1}). ^{1}H (400 MHz) and ^{13}C (100 MHz) NMR spectra were recorded on a Bruker spectrometer at Annamalai University, Annamalai Nagar, India. Chemical shift values are reported in parts per million (ppm) from tetramethylsilane (TMS) as internal standard.

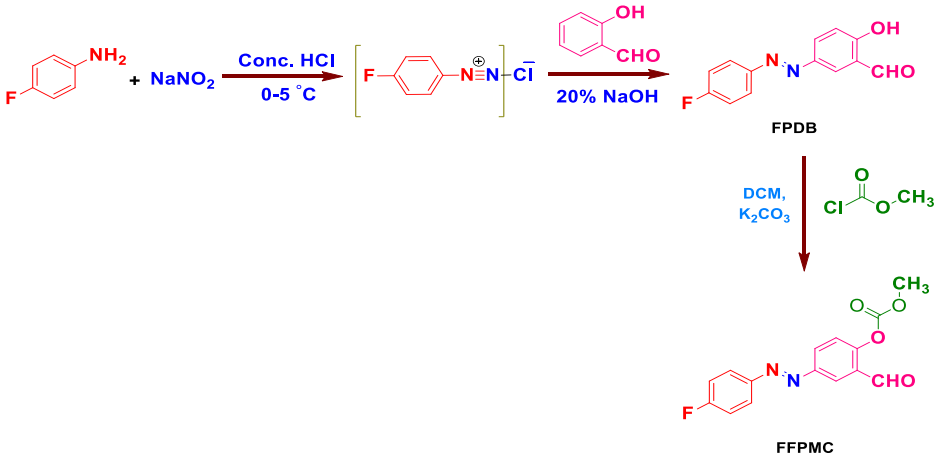

Scheme 1 Synthesis of FFPMC

2.3 Computational details

The entire set of calculations have been performed at HF and DFT–B3LYP methods with 6–31+G(d,p) basis set using *Gaussian 09W* program package [21]. Gradient corrected density functional theory (DFT) has been used with the three parameter hybrid functional (B3) for the exchange part and the

Lee–Yang–Parr (LYP) correlation function [22,23]. The optimized geometry was determined by minimizing the energy with respect to all geometry parameters without imposing molecular symmetry constraints. Besides, the validity of the optimized geometry was confirmed by frequency calculations which gave real values for all the obtained frequencies. The optimized structural parameters were used for the calculation of electronic properties, and isotropic chemical shift calculations. The frequency values computed at these levels contain known systematic errors. Therefore, we have used the scaling factor values of 0.8929 for HF and method 0.9608 for B3LYP [24]. Finally, the calculated normal mode vibrational frequencies provide thermodynamic properties through the principle of statistical mechanics. By combining the results of *GaussView 05* program with symmetry considerations and vibrational frequency assignments were made with high degree of accuracy.

3. RESULTS AND DISCUSSION

3.1 Potential energy surface scan analysis

The most stable geometry of FFPMC was determined through the potential surface scan analysis with B3LYP/6–31+G(d, p) level and the preliminary search of low energy structure was performed for the dihedral angle of C3–C4–N11–N12 which is also a relevant coordinate for conformational flexibility within the molecule. During the calculation, all the geometrical parameters have been simultaneously relaxed with the above dihedral angle which was varied in steps of 10 º from 0 º to 360 º. The potential energy barrier obtained by the rotation of FFPMC with the dihedral angle is shown in Fig. 1.

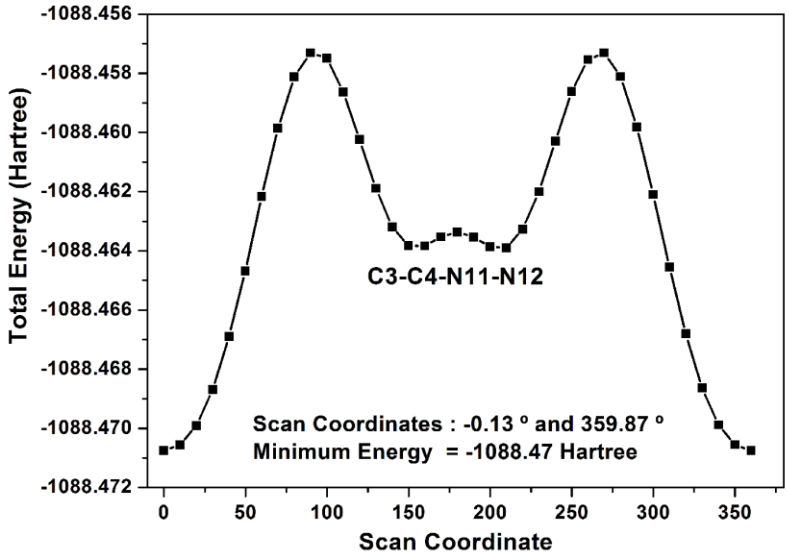

Figure 1. Potential energy surface scan of FFPMC

From Fig. 1, FFPMC attained minimum energy equals -1088.47 a.u at -0.13 º and 359.87 º. The FFPMC showed minimum energy and more stability which is confirmed from the result obtain by potential energy surface scan analysis. From the potential energy surface scan analysis, the optimized geometrical structure of FFPMC is shown in Fig. 2.

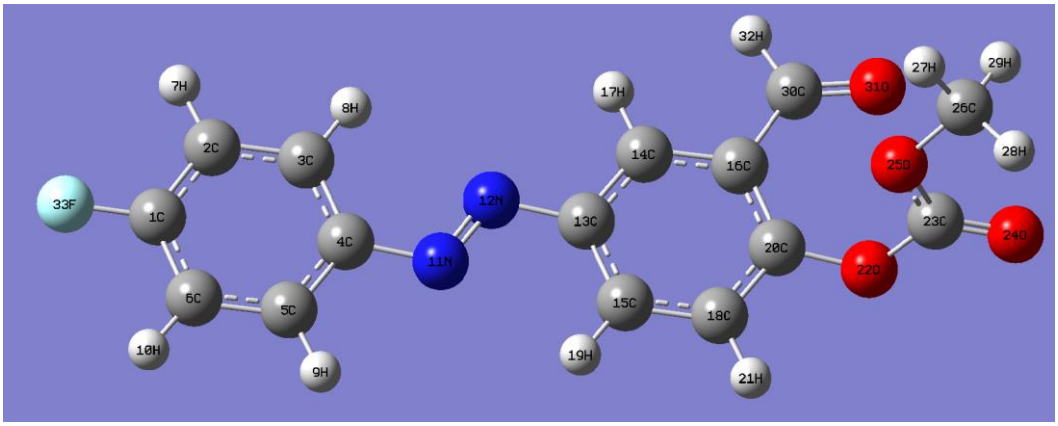

Figure 2. Optimized structure of FFPMC

3.2 Molecular geometry

The molecular structural parameters like bond lengths, bond angles and dihedral angles of FFPMC have been calculated using HF and DFT methods. The calculated structural parameters have been compared with the corresponding crystal structure of azo compounds available in the literature [20,25]. The calculated structural parameters are depicted in Table 1. It is observed from the Fig. 2 and Table 1, that the FPDB basic unit in FFPMC is planar and aromatic in nature due to the continuous delocalization of electrons in the benzene rings through azo group. However, the computed C–H and C–C bond lengths of benzene ring agreed within 0.01–0.02 Å compared to the corresponding literature values. The variations in bond lengths of C4–C5 (1.403/1.402 Å), C13–C14 (1.397/1.381 Å), C16–C30 (1.480/1.459 Å), C16–C20 (1.410/1.415 Å) and C15–C18 (1.39/1.37 Å) are ascribable due to substituent effect, electronegativity and lone pair of electrons present in the molecule. The bond length values of C4–N11 (1.415/1.428 Å) and N12–C13 (1.418/1.425 Å) are found to coincide with related compounds [20]. In FFPMC, an intramolecular hydrogen bond (C–H---O) is present in between O22 and H21 which is confirmed by the result of reduction bond angles equal to 116.5º (C18–C20–O22) and 118.36º (H21–C18–C20) from 120º. Furthermore, the extensions of bond angles are equal to 122.65º (O22–C20–C16) and 124.57º (C20–C16–C30) from 120º. Besides, the dihedral angle of O22–C20–C18–H21 is 4.73º and O22–C20–C16–C30 is -4.70º. This confirmed the presence of intramolecular hydrogen bonding in the molecule.

Table 1. Selected structural parameters for FFPMC

Bond length (Å)	HF	B3LYP	Expt. (Ref [25])	Bond angle (º)	HF	B3LYP	Expt. (Ref [25])	Dihedral angle (º)	HF	B3LYP	Expt. (Ref [25])
C1–C2	1.384	1.395	1.393	C2–C1–C6	122.5	122.8	117.7	C6–C1–C2–C3	0.0	0	-0.9
C1–C6	1.376	1.390	1.398	C2–C1–F33	118.5	118.5	120.9	C6–C1–C2–H7	180.0	180	
C1–F33	1.330	1.356	1.503	C6–C1–F33	118.9	118.8	121.4	F33–C1–C2–C3	180.0	-180	-180
C2–C3	1.381	1.390	1.378	C1–C2–C3	118.8	118.7	121	F33–C1–C2–H7	0.0	0	
C2–H7	1.074	1.085	0.93	C1–C2–H7	119.6	119.6	120.2	C2–C1–C6–C5	0.0	0	0.3

C3–C4	1.394	1.408	1.39	C3–C2–H7	121.6	121.7	118.8	C2–C1–C6–HC10	-180.0	-180	
C3–H8	1.072	1.084	0.96	C2–C3–C4	119.9	120.0	121.4	F33–C1–C6–C5	180.0	180	179.6
C4–C5	1.386	1.403	1.402	C2–C3–H8	120.3	120.8	121.6	F33–C1–C6–HC10	0.0	0	
C4–N11	1.419	1.415	1.428	C4–C3–H8	119.8	119.3	117.3	C1–C2–C3–C4	0.0	0	0.6
C5–C6	1.387	1.394	1.376	C3–C4–C5	120.0	119.9	118.7	C1–C2–C3–H8	180.0	180	
C5–H9	1.075	1.085	0.92	C3–C4–N11	124.4	124.7	126.1	H7–C2–C3–C4	-180.0	-180	
C6–H10	1.074	1.084	0.96	C5–C4–N11	115.6	115.4	115.2	H7–C2–C3–H8	0.0	0	
N11–N12	1.218	1.259	1.259	C4–C5–C6	120.6	120.6	119.7	C2–C3–C4–C5	0.0	0	-1
N12–C13	1.420	1.418	1.425	C4–C5–H9	119.0	118.6	119.2	C2–C3–C4–N11	180.0	-180	178.6
C13–C14	1.383	1.397	1.381	C6–C5–H9	120.4	120.8	121	H8–C3–C4–C5	-180.0	180	
C13–C15	1.392	1.407	1.412	C1–C6–C5	118.2	118.1	121.9	H8–C3–C4–N11	0.0	0	
C14–C16	1.392	1.402	1.396	C1–C6–HC10	120.0	120.0	118.6	C3–C4–C5–C6	0.0	0	0.8
C14–H17	1.076	1.087	0.92	C5–C6–H10	121.8	121.9	119.5	C3–C4–C5–H9	180.0	-180	
C15–C18	1.382	1.390	1.37	C4–N11–N12	116.2	115.5	114.6	N11–C4–C5–C6	180.0	-180	-179
C15–H19	1.073	1.084	0.93	N11–N12–C13	115.7	114.9	113.5	N11–C4–C5–H9	0.0	0	
C16–C20	1.393	1.410	1.415	N12–C13–C14	115.9	115.8	117.1	C3–C4–N11–N12	0.3	0	176.8
C16–C30	1.484	1.480	1.459	N12–C13–C15	124.8	125.0	124.6	C5–C4–N11–N12	-179.7	180	-3.7
C18–C20	1.384	1.397	1.392	C14–C13–C15	119.3	119.1	118.3	C4–C5–C6–C1	0.0	0	0.1
C18–H21	1.074	1.085	0.97	C13–C14–C16	121.6	121.8	122	C4–C5–C6–H10	-180.0	180	
C20–O22	1.366	1.382	1.34	C13–C14–H17	118.5	118.5	120.4	H9–C5–C6–C1	-180.0	-180	
O22–C23	1.335	1.366		C16–C14–H17	119.9	119.8	117.6	H9–C5–C6–H10	0.0	0	
C23–O24	1.180	1.201		C13–C15–C18	119.9	119.9	120.8	C4–N11–N12–C13	-179.9	180	179.4
C23–O25	1.311	1.340		C13–C15–H19	119.8	119.3	120.8	N11–N12–C13–C14	-179.5	180	175.8
O25–C26	1.423	1.444		C18–C15–H19	120.3	120.8	118.4	N11–N12–C13–C15	1.0	0	-4
C26–H27	1.079	1.089		C14–C16–C20	118.2	118.0	118.6	N12–C13–C14–C16	179.8	180	-180
C26–H28	1.080	1.092		C14–C16–	117.7	117.4	120.1	N12–C13–	-0.3	-1	

				C30				C14–H17			
C26–H29	1.080	1.092		C20–C16–C30	124.1	124.6	121.3	C15–C13–C14–C16	-0.7	-1	-0.2
C30–O31	1.191	1.218	1.219	C15–C18–C20	120.4	120.5	120.7	C15–C13–C14–H17	179.3	179	
C30–H32	1.094	1.111	0.97	C15–C18–H21	120.9	121.1	120.1	N12–C13–C15–C18	179.8	180	-179
				C20–C18–H21	118.7	118.4	119.1	N12–C13–C15–H19	0.1	0	
				C16–C20–C18	120.6	120.6	119.6	C14–C13–C15–C18	0.3	0	1.1
				C16–C20–O22	122.2	122.7	122.7	C14–C13–C15–H19	-179.4	-179	
				C18–C20–O22	116.9	116.5	117.7	C13–C14–C16–C20	0.3	0	-0.7
				C20–O22–C23	123.4	122.7	106	C13–C14–C16–C30	-179.8	179	179.2
				O22–C23–O24	121.3	121.4		H17–C14–C16–C20	-179.7	-180	
				O22–C23–O25	112.3	111.5		H17–C14–C16–C30	0.3	-1	
				O24–C23–O25	126.3	127.0		C13–C15–C18–C20	0.6	0	-1.1
				C23–O25–C26	116.5	114.9		C13–C15–C18–H21	-179.0	-179	
				O25–C26–H27	105.4	105.2		H19–C15–C18–C20	-179.8	-180	
				O25–C26–H28	110.2	110.2		H19–C15–C18–H21	0.6	1	
				O25–C26–H29	109.8	109.8		C14–C16–C20–C18	0.6	1	0.7
				H27–C26–H28	110.7	110.9		C14–C16–C20–O22	174.7	174	-179
				H27–C26–H29	110.7	110.9		C30–C16–C20–C18	-179.4	-178	-179
				H28–C26–H29	110.0	109.9		C30–C16–C20–O22	-5.3	-5	1
				C16–C30–O31	125.7	126.2	122.7	C14–C16–C30–O31	171.4	175	176.5
				C16–C30–H32	114.0	113.6	114.1	C14–C16–C30–H32	-8.1	-5	
				O31–C30–H32	120.3	120.3	122.2	C20–C16–C30–O31	-8.6	-6	-3.5
								C20–C16–C30–H32	171.9	174	
								C15–C18–C20–C16	-1.0	-1	0.2
								C15–C18–C20–O22	-175.4	-175	179.9
								H21–C18–C20–C16	178.6	179	

H21–C18–C20–O22	4.2	5
C16–C20–O22–C23	74.6	69
C18–C20–O22–C23	-111.1	-118
C20–O22–C23–O24	-175.0	-172
C20–O22–C23–O25	7.9	12
O22–C23–O25–C26	-176.4	-177
O24–C23–O25–C26	6.6	7
C23–O25–C26–H27	179.7	-179
C23–O25–C26–H28	-60.9	-60
C23–O25–C26–H29	60.4	61

The dihedral angle between the two benzene rings C4–N11–N12–C13 (C4 through C13) is 180º. However, the C16–C20–O22–C23 and C18–C20–O22–C23 planes are inclined by 69º and -118º in the skeleton from the molecular plane. The structural parameter data obtained from computed methods are in good agreement with the literature values [20,25].

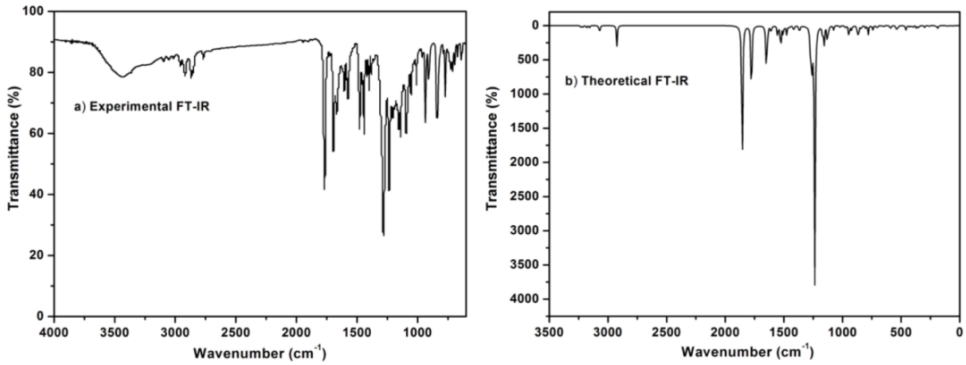

Figure 3. (a) Experimental FT–IR and (b) Theoretical FT–IR spectra of FFPMC

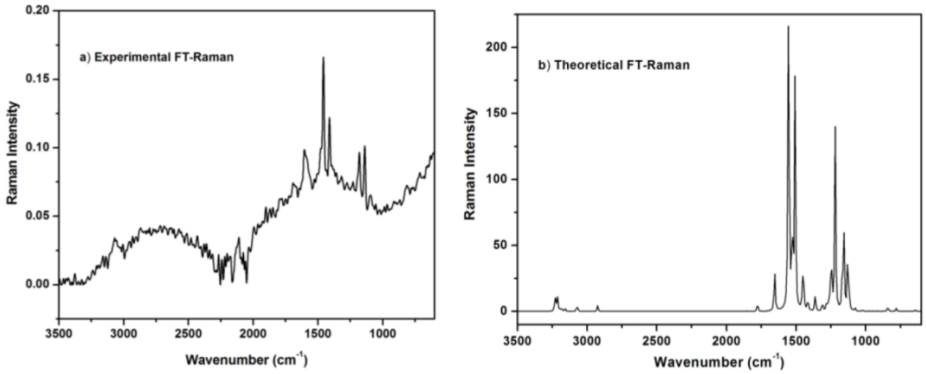

Figure 4. (a) Experimental FT–Raman and (b) Theoretical FT– Raman spectra of FFPMC

3.3 Vibrational analysis

Vibrational analysis were performed by B3LYP/6-31+G(d,p) level and it provides the symmetry, mode numbers, Infrared frequency, Raman intensity, reduced mass and force constants of the compound. We get the types of vibrations and vibrational assignments using Veda 4e1 (Vibration energy distribution analysis) software. FFPMC has 33 atoms, belongs to C1 symmetry and possesses 93 normal modes of vibration. All the 93 modes of vibrations are distributed as 32 stretching, 31 in–planes, 24 torsional and 6 out–of–plane vibrations in the infrared spectrum. The experimental and calculated scaled frequencies as well as the TED are listed in Table 2. The calculated frequencies of the investigated molecules are very close to the corresponding literature values. The mean percentage deviations of the calculated frequencies from the experimental ones are about 1.0–2.0 %.

3.3.1 C=O vibrations

The C=O stretching vibrational band can be easily identified from the FT–IR and FT–Raman spectra, because of the degree of conjugation, strength and polarizations. The carbonyl stretching vibrations are expected in the region between 1715–1680 cm^{-1} [19,20,26]. In FFPMC, two C=O stretching bands are observed in both experimental FT–IR and FT–Raman spectra, one C=O stretching bands are observed at 1768 cm^{-1} for carbonate and another at 1695 cm^{-1} for aldehyde in FT–IR spectrum, while in FT–Raman spectrum the carbonate C=O stretching band observed at 1768 cm^{-1} and the C=O stretching of aldehyde at 1692 cm^{-1}.

Table 2. Experimental and calculated vibrational spectral values of FFPMC with proposed assignment

Mode No	Observed frequency (cm^1)		Calculated Frequeny (cm^1)		Intensity		Red. mass	Force constant	Vibrational Assignments with TED ≥ 10%
	FT-IR	Raman	Un Scaled	Scaled	IR	Raman			
1			20	20	1.77	2.69	4.08	0	τN12N11C4C3 (36) + τC16C14C13C15 (51)
2			26	25	2.29	1.54	7.19	0	τC16C14C13C15 (21) + τC13N12N11C4 (26) + ΓC15C14CN12C13 (18)
3			45	43	2.27	1.91	5.93	0	βN12N11C4 (10) + βC13N12N11 (11) + τC23O22C20C16 (33) + τO25C23O22C20 (10)
4			57	55	3.77	1.5	6.49	0	βN12N11C4 (11) + βC13N12N11 (10) + τO25C23O22C20 (13)
5			67	65	3.34	2.21	5.48	0	τΓ25C23Γ22C20 (31) + ΓN11C3C5C4 (10)
6			83	80	2.35	1.22	5.34	0	τC23O22C20C16 (37) + τO25C23O22C20 (16)
7			98	95	3.44	1.05	7.48	0	βO22C20C18 (13) + τO31C30C16C14 (12) + τN12N11C4C3 (14)
8			110	106	5.2	1.37	4.76	0	τO31C30C16C14 (17) +

								τC26O25C23O22 (23)
9		130	125	1.76	0.83	1.22	0	τH29C26O25C23 (58)
10		175	169	3.49	1.51	7.92	0	νN12C13 (11) + βN12N11C4 (10) + βN11C4C5 (11)
11		187	180	7.44	1.09	5.38	0	βC30C16C14 (17) + τO31C30C16C14 (16) + τC26O25C23O22 (13)
12		189	182	7.35	1.1	4.28	0	τC16C14C13C15 (13) + τC26O25C23O22 (19)
13		200	193	5.62	0.86	6.96	0	νN12C13 (10) + βC30C16C14 (25) + τC26O25C23O22 (13)
14		207	200	4.34	1.02	10.25	0	τN12N11C4C3 (17) + τC4C5C6C1 (38) + ΓF33C1C2C6 (12)
15		262	253	4.72	3.35	6.97	0	βC14C13N12 (15) + βN11C4C5 (12)
16		263	254	3.09	1.4	3.42	0	ΓC30C14C20C16 (32)
17		301	290	8.67	2.52	4.76	0	βC26O25C23 (44)
18		352	340	11.29	1.62	8.89	1	νO22C20 (10)
19		371	358	10.13	3.41	6.47	1	ΓC15C14CN12C13 (13) + ΓN11C3C5C4 (13)
20		399	385	8.63	1.78	8.15	1	βF33C1C6 (42)
21		410	395	5.47	0.93	4.73	0	τC2C1C6C5 (15) + τC3C2C1C6 (17) + τC13N12N11C4 (11) + ΓF33C1C2C6 (14)
22		427	412	6.84	0.88	6.04	1	βO31C30C16 (12) + βO22C20C18 (14) + βO22C20C18 (22) + βF33C1C6 (17)
23		438	422	3.17	0.68	3.71	0	τC2C1C6C5 (58)
24		457	441	10.05	3.61	4.71	1	τC16C14C13C15 (25)
25	469	460	444	10.44	2.42	5.69	1	βC1C2C6 (13) + τC16C14C13C15 (15)
26	501	524	505	6.88	1.18	2.66	0	τH9C5C6C1 (14) + ΓF33C1C2C6 (23) + ΓN11C3C5C4 (19)
27		537	518	14.99	4.85	6.71	1	βN12N11C4 (16) + βN11C4C5 (11)
28	550	547	527	5.12	5.78	6.97	1	βC16C14C13 (13) + βC13N12N11 (12)
29	580	591	570	12.65	2.05	3.98	1	τC13N12N11C4 (11) + ΓC30C14C20C16 (12) + ΓC15C14CN12C13 (20)

30			643	620	2.66	5.22	5.80	1	βC1C6C5 (10) + βC4C5C6 (31)
31			647	624	5.83	2.82	5.17	1	βC4C5C6 (18) + βC15C13C14 (15)
32	640		664	641	5.22	2.62	7.19	2	βO24C23O25 (16)
33	670		704	679	11.15	1.4	6.71	2	βO31C30C16 (17) + βC18C15C13 (13)
34	699	693	718	693	4.22	3.06	4.34	1	τC3C2C1C6 (38) + ΓF33C1C2C6 (12) + ΓN11C3C5C4 (12)
35	711		740	714	12.84	1.92	7.13	2	ΓO24O22O25C23 (57)
36	724		755	728	5.31	2.81	5.37	2	βO24C23O25 (10) + ΓO24O22O25C23 (22) + ΓO22C16C18C20 (10)
37		749	780	753	18.66	8.32	5.70	2	βO31C30C16 (16) + βC18C15C13 (19)
38	771		805	776	10.05	2	5.66	2	τN12N11C4C3 (10) + τO31C30C16C14 (32) + βC13N12N11 (12) + βC18C15C13 (23)
39			827	798	0.87	0.41	1.24	1	τH7C2C1C6 (20) + τH8C3C4C5 (30) + τH9C5C6C1 (19) + τH10C6C1C2 (31)
40			841	811	12.03	11.32	6.17	3	νC6C5 (21) + νF33C1 (10)
41	834	835	863	833	18.63	1.11	1.64	1	τH7C2C1C6 (19) + τH8C3C4C5 (11) + τH9C5C6C1 (10) + τH10C6C1C2 (10) + τC4C5C6C1 (13) + ΓF33C1C2C6 (15)
42			872	841	19.96	2.83	1.61	1	τH19C15C18C20 (24) + τH17C14C16C20 (41) + ΓO22C16C18C20 (10)
43			913	881	6.43	4.47	6.25	3	νC6C5 (19) + βC13N12N11 (13)
44			926	893	13.31	1.55	1.45	1	τH19C15C18C20 (30) + τH21C18C20C16 (13) + τH17C14C16C20 (18) + τC16C14C13C15 (13)
45	910		945	912	23.08	3.47	6.08	3	νO22C20 (18) + νO25C26 (14) + βO25C23O22 (12)
46	935	931	967	933	1.5	0.99	1.32	1	τH8C3C4C5 (38) + τH9C5C6C1 (28) + τH10C6C1C2 (10) + τC4C5C6C1 (12)
47			975	941	10.41	4.25	4.46	2	νC20C18 (10) + νC15C13 (10) + νC16C14 (15)

48			985	950	0.09	0.14	1.33	1	τH7C2C1C6 (38) + τH9C5C6C1 (14) + τH10C6C1C2 (35)
49		962	995	961	1.64	0.9	1.35	1	τH17C14C16C20 (34) + τH21C18C20C16 (42) + τC16C14C13C15 (13)
50			1023	987	11.83	7.87	1.80	1	τH17C14C16C20 (38) + τH19C15C18C20 (12) + τH21C18C20C16 (19) + τH17C14C16C20 (13)
51	1010	1012	1023	987	11.83	7.87	2.47	2	βC1C6C5 (16) + βH10C6C1 (23) + βC1C6C5 (45)
52	1053	1049	1077	1039	13.24	8.16	8.76	6	νO22C20 (18) + νO25C26 (58)
53			1116	1077	10.17	12.2	1.26	1	νC2C1 (15) + βH9C5C6 (66)
54	1094	1092	1129	1089	27.76	41.1	1.54	1	νC18C15 (15) + βH17C14C16 (24) + βH21C18C20 (11)
55			1158	1118	30.89	49.25	1.29	1	νC3C2 (13) + βH8C3C2 (60)
56			1171	1130	16.2	23.85	1.48	1	βH8C3C2 (11) + βH19C15C18 (37)
57	1141	1140	1178	1137	3.95	3.1	1.27	1	βH28C26H27 (27) + τH27C26O25C23 (25) + τH28C26O25C23 (27) + τH29C26O25C23 (18)
58	1154		1214	1172	4.04	5.77	1.50	1	βH27C26H29 (24)+ τH27C26O25C23 (31) + τH28C26O25C23 (30)
59		1182	1220	1177	13.41	67	3.54	3	νN12C13 (22) + νC30C16 (11) + βH10C6C1 (12) + βC1C6C5 (12)
60		1199	1237	1193	100	5.43	6.08	5	νO22C23 (65)
61	1205		1248	1204	26.01	40.04	4.67	4	νF33C1 (27)
62			1259	1215	38.45	14.81	4.39	4	νC6C5 (12) + νO22C20 (19) + νF33C1 (14) + βH17C14C16 (12)
63		1227	1271	1227	44.5	13.13	6.32	6	νO22C20 (22) + νN11C4 (19)
64	1235		1282	1237	8.13	12.17	1.62	2	βH17C14C16 (27) + βH19C15C18 (13) + βH21C18C20 (17)
65	1282	1262	1312	1266	3.56	15.47	1.33	1	νC5H9 (86)
66	1316	1303	1362	1315	10.99	20.1	10.90	12	νC1C6 (49) + νC4C5 (22)
67			1370	1322	13.17	6.44	10.06	11	νC4C5 (35) + νC20C18 (12)

68	1381		1416	1366	16.22	18.14	1.79	2	νC18C15 (10) + νC15C13 (12) + βH32C30O31 (45)
69	1399	1397	1448	1398	6.74	36.94	3.61	4	νC1C6 (14) + νC2C1 (28) + βH9C5C6 (27)
70			1456	1405	9.19	16.1	2.12	3	νC15C13 (12) + βH32C30O31 (40)
71	1416	1414	1476	1424	18.4	2.48	1.18	2	βH29C26H28 (81)
72			1489	1437	8.61	4.56	1.05	1	βH28C26H27 (69) + τH28C26O25C23 (15)
73			1502	1449	7.17	13.69	1.06	1	βH27C26H29 (62) + τH27C26O25C23 (14)
74	1442	1449	1508	1455	16.66	77.25	2.75	4	νN12N11 (12) + βH21C18C20 (33)
75			1528	1474	33.4	50.19	2.91	4	βH10C6C1 (32) + βH21C18C20 (10)
76	1478	1483	1554	1499	21.43	100	6.05	9	νN12N11 (53)
77			1609	1552	17.34	3.47	7.59	12	νC15C13 (28)
78	1574	1583	1636	1579	14.02	2.75	7.55	12	νC1C6 (10) + νC2C1 (26) + βC1C6C5 (11) + βC4C5C6 (11)
79	1606	1601	1648	1591	45.96	9.61	6.32	10	νC3C2 (37) + νC14C13 (18) + βH8C3C2 (14)
80	1667		1654	1596	18.95	35.39	6.69	11	νC14C13 (22) + βH17C14C16 (11)
81	1695	1692	1776	1714	60.79	16.41	10.14	19	νO24C23 (46) + νO31C30 (40)
82	1768	1768	1855	1790	85.12	5.01	12.03	24	νO24C23 (39) + νO31C30 (47)
83	2868	2869	2924	2821	28.21	14.73	1.08	5	νC14H17 (25) + νC15H19 (24) + νC18H21 (26) + νC14H17 (24)
84	2965	2958	3072	2964	18.58	16.79	1.03	6	νC26H29 (94)
85	3011	3050	3158	3047	9.66	10.86	1.11	7	νC26H27 (46) + νC26H28 (54)
86	3049	3065	3182	3070	9.12	9.77	1.11	7	νC26H27 (51) + νC26H28 (43)
87			3193	3081	3.06	8.5	1.09	7	νC14H17 (28) + νC15H19 (26) + νC18H21 (21) + νC14H17 (25)
88			3210	3098	4.58	9.84	1.09	7	νC3H8 (65) + νC6H10 (25)
89	3094		3211	3099	4.87	15.6	1.09	7	νC14H17 (36) + νC18H21 (43) + νC14H17 (12)
90			3215	3102	4.65	17.93	1.09	7	νC3H8 (22) + νC6H10 (60) + νC14H17 (11)

91		3226	3113	6.05	20.5	1.10	7	νC2H7 (48) + νC14H17 (42)
92		3232	3119	4.42	12.51	1.09	7	νC14H17 (10) + νC15H19 (40) + νC18H21 (11) + νC14H17 (39)
93	3440	3233	3119	5.94	11.33	1.09	7	νC2H7 (39) + νC6H10 (10) + νC14H17 (43)

ν – stretching, β – in-plane bending, τ – torsional vibrations, Γ – out of plane bending.

From the DFT calculation, the carbonate C=O stretching band observed at 1790 cm^{-1} and the C=O stretching of aldehyde at 1714 cm^{-1} (mode nos. 81, 82) (In parent compound at 1768 cm^{-1} for the carbonate C=O and 1788 cm^{-1} for aldehyde [27]) which are correlated with the experimental FT–IR and FT–Raman values. The experimental FT–IR and FT–Raman spectra with the corresponding theoretically simulated ones are shown in Figs. 3 and 4.

3.3.2 C–C and C=C vibrations

The ring carbon atoms undergo coupled vibrations, known as semicircular stretching usually occurring in the region 1400–1625 cm^{-1}. The actual positions of these modes are determined not so much by the nature of the substituent but by the form of substitution around the ring [26,28]. In the experimental FT–IR spectrum, C–C vibration band was observed with stretching frequency at 1316 cm^{-1}, in FT–Raman band at 1303 cm^{-1} and stretching with in–plane bending frequency at 1399 cm^{-1} (FT–IR), 1397 cm^{-1} (FT–Raman) and 1398 cm^{-1} (mode no. 69). The theoretically computed stretching frequency in B3LYP/6–31+G(d,p) method were predicted at 1552, 1322 and 1315 cm^{-1} (mode nos. 77, 67, and 66). Most of the theoretical modes of vibrations are closed to the experimental frequencies.

3.3.3 C–H vibrations

The C–H stretching vibrations in aromatic ring appear above 3000 cm^{-1} which is the characteristic region for the ready identification of such C–H stretching vibrations [26,28] and are typically exhibited as a multiplicity of weak to moderate bands [29]. In FFPMC, eleven C–H stretching vibrations are assigned which are represented as mode nos. 83–93 for both the benzene rings and carbonate methyl group C–H. The mode nos. 87–93 assigned to symmetric C–H stretching vibrations of benzene rings and remaining five modes (mode nos. 83–87) for carbonate methyl group C–H asymmetric vibrations. From B3LYP/6–31+G(d,p) method the harmonic frequencies of both benzene rings are occurs in between 3073–3118 cm^{-1} and the aromatic C–H in–plane bending vibrations occur in the region at 1398–987 cm^{-1} with the mode nos. 69–51 which are sharp but weak to medium intensity. The C–H in–plane bending harmonic vibrations are observed in experimental FT–IR at 1399, 1235, 1094 and 1010 cm^{-1}. In experimental FT–Raman, bands are observed at 1397, 1092, and 1012 cm^{-1} and their the C–H in–plane bending vibrations computed at 1398, 1237, 1118, 1077, 1089 and 987 cm^{-1} corresponding mode nos. 69, 64, 55, 57, 53 and 51, respectively. Beside the C–H in–plane bending vibration observed at 1416 cm^{-1} in FT–IR and 1414 cm^{-1} in FT–Raman corresponds to the mode no. 71. The computed values showed a good agreement with medium and strong FT–IR and FT–Raman bands. The computed values of C–H in–plane and out–of–plane bending vibrations are listed in Table 2.

3.3.4 Methyl group vibrations

The asymmetric stretching vibrations of CH_3 are expected to appear at about 2980 cm^{-1} and symmetric stretching vibrations around 2800–2870 cm^{-1} [30,31]. The strong bands are observed in FT–IR spectrum between 3438–3027 cm^{-1} which are assigned as C–H asymmetric stretching and C–H symmetric stretching of CH_3 are observed at 3049, 3011 and 2965 cm^{-1}. In FT–Raman spectrum, C–H stretching frequencies at 3065, 3050 and 2958 cm^{-1} and in computed, C–H stretching frequencies appeared at 3070, 3047 and 2964 cm^{-1} (mode nos. 86–84), respectively. All these assignments are in good agreement with literature values. Furthermore, the stretching frequency of N12–N13 is observed in FT–IR at 1478 cm^{-1} and FT–Raman at 1483 cm^{-1}. The theoretical N–N stretching observed at 1499 cm^{-1} (mode no. 76) which is close to the experimental value.

3.4 Mulliken Population analysis

Mulliken population analysis provides the atomic charge density or an orbital density on individual atom. Atomic charge density of compound FFPMC obtained by Mulliken population using HF and B3LYP levels with 6–31+G(d,p) basis set.

The net Mulliken atomic charge values are listed in Table 3 and Mulliken charge distribution is shown in Fig. 5. The charge distributions over the atoms suggest the formation of donor and acceptor pairs involving the charge transfer in the molecule [32,33]. The magnitude of carbon atom attached at nitrogen atoms have attained highest negative charge and behaved as electron acceptors, whereas the large accumulation of positive charge on carbon atoms (16C/15C) than the other atoms.

Table 3 Mulliken atomic charges of FFPMC

Atoms	Charges	
	HF	B3LYP
C1	-0.237	0.008
C2	0.010	0.037
C3	0.210	0.393
C4	-0.912	-0.770
C5	0.477	-0.042
C6	0.075	0.107
H7	0.197	0.144
H8	0.200	0.155
H9	0.183	0.141
H10	0.197	0.145
N11	0.053	0.053
N12	-0.009	-0.046
C13	-0.979	-1.088
C14	-0.260	-0.136
C15	0.515	0.496
C16	0.798	0.760
H17	0.191	0.143
C18	0.333	-0.075
H19	0.206	0.157
C20	-0.882	-0.527

H21	0.196	0.140
O22	-0.507	-0.287
C23	0.909	0.472
O24	-0.547	-0.457
O25	-0.431	-0.226
C26	-0.078	-0.159
H27	0.137	0.157
H28	0.150	0.188
H29	0.152	0.161
C30	0.385	0.476
O31	-0.453	-0.317
H32	0.125	0.129
F33	-0.403	-0.332

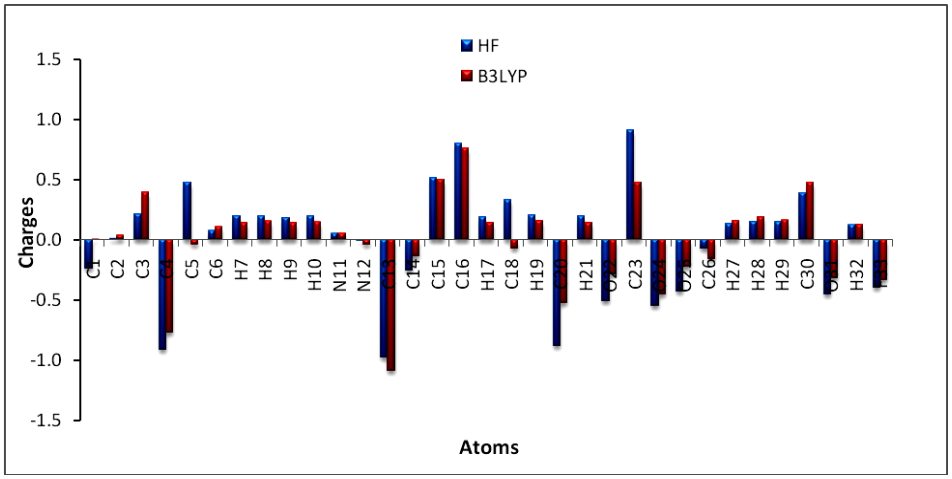

Figure 5. Mulliken charge distribution of FFPMC

3.5 NBO analysis

NBO analysis was performed using the *Gaussian 09W* package at the B3LYP/6–31+G(d,p) level in order to understand the various second–order interactions between the filled orbitals of one subsystem and vacant orbitals of another subsystem, which is a measure of the intermolecular delocalization or hyperconjugation [34]. The second order Fock matrix was carried out to evaluate the donor–acceptor interactions in the NBO basis [35]. For each donor (i) and acceptor (j), the stabilization energy $E^{(2)}$ associated with the delocalization is estimated as:

$$E^{(2)} = \Delta E_{ij} = q_i \frac{F(i,j)^2}{\varepsilon_j - \varepsilon_i}$$

where q_i is the donor orbital occupancy, $\mathcal{E}_i$ and $\mathcal{E}_j$ are diagonal elements and $F_{i,j}$ is the off diagonal NBO Fock matrix element. A larger $E^{(2)}$ value indicates a more intense interaction between electron donors and electron acceptors which leads to a greater extent of conjugation in the system

In the present investigation, transfer of charges from bonding to antibonding level has been studied. The maximum charge delocalization occurs from the lone pairs of electrons. The strong intramolecular hyperconjugative interaction of π electrons occurs from C1–C6, C2–C3 and C4–C5

bonds to the π*(C1–C6) bond of the benzene (1) ring which increases the ED (0.3634 eV) leading to stabilization of 22.97 kJ/mol.

Table 4 Second order perturbation theory analysis of Fock matrix in NBO basis for FFPMC

Type	Donor (i)	ED (i)(e)	Acceptor (j)	ED (j)(e)	[a]E(2) kcal/mol	[b]E(j)–E(i) a.u	[c]F(i,j) a.u.
π–π*	C1 – C6	1.6485	C4 – C5	0.379	21.85	0.29	0.072
σ–σ*		1.9727	C1 – F33	0.0319	4.43	0.96	0.058
π–π*	C2 – C3	1.6914	C1 – C6	0.3634	22.97	0.28	0.072
π–π*		1.6914	C4 – C5	0.379	17.07	0.28	0.063
π–π*	C4 – C5	1.6137	C2 – C3	0.2916	20.43	0.28	0.069
π–π*		1.6137	N11 – N12	0.216	21.19	0.23	0.065
σ–σ*	C4 – N11	1.9808	N12 – C13	0.0286	4.13	1.2	0.063
π–π*	N11 – N12	1.9133	C13 – C14	0.3523	10.45	0.39	0.061
σ–σ*	N12 – C13	1.9806	C4 – N11	0.0279	4.23	1.2	0.064
σ–σ*	C13 – C14	1.9772	C16 – C30	0.0594	2.71	1.15	0.05
π–π*	C13 – C14	1.6122	C15 – C18	0.2787	20.24	0.28	0.07
π–π*	C15 – C18	1.6549	C16 – C20	0.4128	24.07	0.27	0.074
σ–σ*	C16 – C20	1.9748	C14 – H17	0.0159	2.09	1.18	0.045
π–π*		1.6014	C13 – C14	0.3523	22.28	0.29	0.072
π–σ*	C23 – O24	1.9924	C20 – O22	0.0341	1.47	1.05	0.035
σ–σ*	O25 – C26	1.9865	O22 – C23	0.1142	3.93	1.16	0.062
π–π*	C30 – O31	1.9785	C16 – C20	0.4128	4.6	0.39	0.042
n – σ*	LP(1) N11	1.95038	C3 – C4	0.0328	8.61	0.96	0.081
n – σ*	LP(1) N11	1.95018	C13 – C15	0.03336	8.8	0.96	0.082
n – π*	LP(1) O22	1.92461	C16 – C20	0.41282	6.07	0.56	0.057
n – σ*	LP(1) O22	1.92461	C23 – O25	0.10633	6.48	0.92	0.07
n – σ*	LP(2) O22	1.8274	C23 – O24	0.15551	12.05	0.67	0.08
n – σ*	LP(2) O24	1.81371	O22 – C23	0.11424	33.72	0.59	0.129
n – σ*	LP(2) O24	1.81371	C23 – O25	0.10633	31.14	0.62	0.127
n – σ*	LP(1) O25	1.95632	C23 – O24	0.15551	7.53	0.91	0.076
n – σ*	LP(2) O25	1.81257	C23 – O24	0.15551	10.53	0.66	0.075
n – π*	LP(2) O25	1.81257	C23 – O24	0.1685	15.38	0.63	0.088
n – σ*	LP(2) O31	1.88033	C16 – C30	0.05947	19.43	0.71	0.106
n – σ*	LP(2) O31	1.88033	C30 – H32	0.06116	21.4	0.67	0.108
n – π*	LP (3) F33	1.9201	C1 – C6	0.36348	19.1	0.43	0.087
π*–π*	N11 – N12	0.21608	C4 – C5	0.37906	28.21	0.05	0.059
π*–π*	N11 – N12	0.21608	C13 – C14	0.35232	28.28	0.04	0.058
σ*–σ*	O22 – C23	0.11424	C23 – O25	0.10633	0.99	0.03	0.014
σ*–σ*	C23 – O24	0.15551	O22 – C23	0.11424	16.83	0.01	0.037
σ*–σ*	C23 – O24	0.15551	C23 – O25	0.10633	10.61	0.04	0.052
π*–σ*	C23 – O24	0.1685	C23 – O24	0.15551	653.52	0.03	0.306

[a] Energy of hyper conjugative interaction (stabilization energy), [b] Energy difference between donor and acceptor i and j NBO orbitals, [c] F(i,j) is the fock matrix element between i and j NBO orbitals.

Furthermore, the π-electron delocalization is maximum around the C13–C14, C15–C18, C16–C20 of the benzene (2) ring which increases the ED (0.4128 eV) leading to stabilization of 24.07 kJ/mol. According to the NBO second-order perturbation, estimation of the interaction energies between donor and acceptor π–NBOs, there is considerable resonance effect in the molecule operating between its azo group and the two benzene rings. The interaction energy between the filled bond orbital π(N11–N12) and the empty anti-bond π*(C–C) orbital of benzene (1) and benzene (2) rings are 10.01 and 10.45 kJ/mol, respectively, as shown in Table 4. Therefore, the lone pair electrons of the azo group are not involved in localization since lone pairs lie in the molecular plane which is orthogonal to the π system. The azo group being co-planar with the benzene (2) ring increases the conjugation between them which supports electron delocalization from azo group to the benzene (2) ring which is revealed by the high value of the interaction energy is equal to 28.28 kJ/mol. These intramolecular charge transfer (n→π*, π→ π* and π*→π*) can induce large non linearity to the molecule.

The most important interaction energy, related to the resonance in the molecule, is electron donation from LP(1) O22 to the anti-bonding acceptor π*(C16–C20) of the benzene (2) ring is equivalent to 6.07 kJ/mol which is lower compared than LP(2) O22 to anti-bonding acceptor σ*(C23–O24) which is almost equal to 12.05 kJ/mol. Furthermore π*(C23–O24) to σ*(C23–O24) results in a stabilization energy value of 653.52 kJ/mol whereas (*E*)-5-(2-phenyldiazenyl)-2-hydroxybenzaldehyde posses higher values equals to 1104.14 [27]. Therefore electrons of LP(2) O22 is preferred to delocalization towards C23–O24 and not for benzene (2) ring. These NBO results confirmed that the lone pair electron interaction is not present in between the oxygen (O22) of the carbonate group and benzene (2) ring or benzene (2) ring with aldehyde group.

3.6 HOMO–LUMO analysis

The HOMO and LUMO are important quantum chemical parameters to determine the molecular interaction with other species and to characterize the chemical reactivity, global hardness, softness and kinetic stability of the molecule etc. [36]. E_{HOMO} is often associated with the electron–donating ability of a molecule, while E_{LUMO} indicates its ability to accept electrons. Due to the interaction between HOMO and LUMO orbital of a structure, π–π* and n–π* transition state is observed with regard to the molecular orbital theory [36]. The frontier orbital gap aids to characterize the chemical reactivity and kinetic stability of the molecule. Therefore, the energy of the HOMO is directly related to the ionization potential and LUMO energy is directly related to the electron affinity. However, a molecule with a small frontier orbital gap is generally associated with a high chemical reactivity and low kinetic stability. The 3D plots of HOMOs and LUMOs are calculated using HF and B3LYP/6–31+G (d,p) methods which are shown in Fig.6 and the energy gap between HOMO and LUMO orbitals is given in Table 5.

According to Fig. 6, the HOMO orbital is localized over the nitrogen and carbon atoms of C3, C4, C13 and C14 while the LUMO is characterized by a charge distribution over entire molecule except –OCH3 part of carbonate. Moreover a small in the HOMO and LUMO energy gap (2.191eV) due to fluorine atom influences the energy gap of molecule which explains the eventual charge transfer interactions occurring within the molecule.

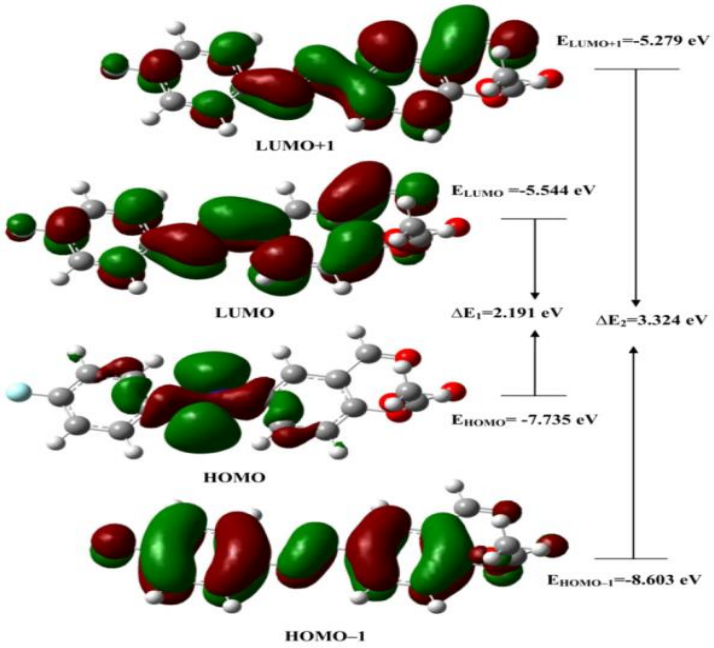

Figure 6. HOMO–LUMO plot of FFPMC using B3LYP method

Using HOMO and LUMO orbital energies, the ionization energy, electron affinity and related properties can be expressed as [37]:

$$IP = -E_{HOMO} = 8.134 \text{ eV}, \qquad EA = -E_{LUMO} = 7.735 \text{ eV},$$

$$\eta = -(E_{HOMO} + E_{LUMO})/2 = -6.64 \text{ eV}, \qquad \chi = (E_{LUMO} - E_{HOMO})/2 = 1.095 \text{ eV}.$$

Table 5. Calculated HOMO–LUMO energies of FFPMC

Energy	HF (eV)	B3LYP (eV)
E_{HOMO}	-8.134	-7.735
E_{LUMO}	-5.635	-5.544
ΔE_1	2.679	2.191
E_{HOMO-1}	-8.611	-8.603
E_{LUMO+1}	-5.241	-5.279
ΔE_2	3.37	3.324

3.7 NMR spectral analysis

NMR spectroscopy is a powerful tool to predict and interpret the structure of molecules. ^{1}H NMR spectrum gives the information about the various kinds of protons as well as their orientation in different environments. ^{13}C NMR spectrum provides the structural information with regard to different carbon atoms present in molecules. It is recognized that accurate prediction of molecular geometries are essential for reliable calculation of magnetic properties. The ^{1}H and ^{13}C chemical shifts calculation of FFPMC have been made by HF and B3LYP with 6–31+G(d,p) basis set [38,39] and compared with the experimental values and are presented in Table 6 and Fig. 7, respectively.

In experimental ^{1}H NMR, one signal observed in upfield region at 3.99 ppm (s) with three proton integral corresponds to H27, H28 and H29 atoms respectively. In the downfield region the signals at 10.27 (s), 8.43 (s), 8.19 (d) and 7.47 (d) ppm corresponds to H32, H17, H19 and H21 atoms, respectively. The experimental chemical shift values were found to be consistent with the computed values of 3.745, 4.304,

4.109, 10.776, 9.053, 9.053 and 7.853 ppm with HF and B3LYP/6–31+G(d,p) level for H27, H28, H29, H32, H17, H19 and H21, atoms, respectively. The root mean square values for proton chemical shifts were found to be 0.995 and standard deviation was 0.226 for B3LYP/6–31+G(d,p) basis set.

In experimental ^{13}C NMR, signals for aromatic carbons of the FFPMC are observed at 166.1 (C1), 123.8 (C2), 116.4 (C3), 128.5 (C5), 116.2 (C6), 129.1 (C14), 125.2 (C15), 125.3 (C16) and 125.3 (C18) ppm, respectively. The shielded signal at 56.1 ppm is assigned to the carbonate methyl carbon (C26) [40].

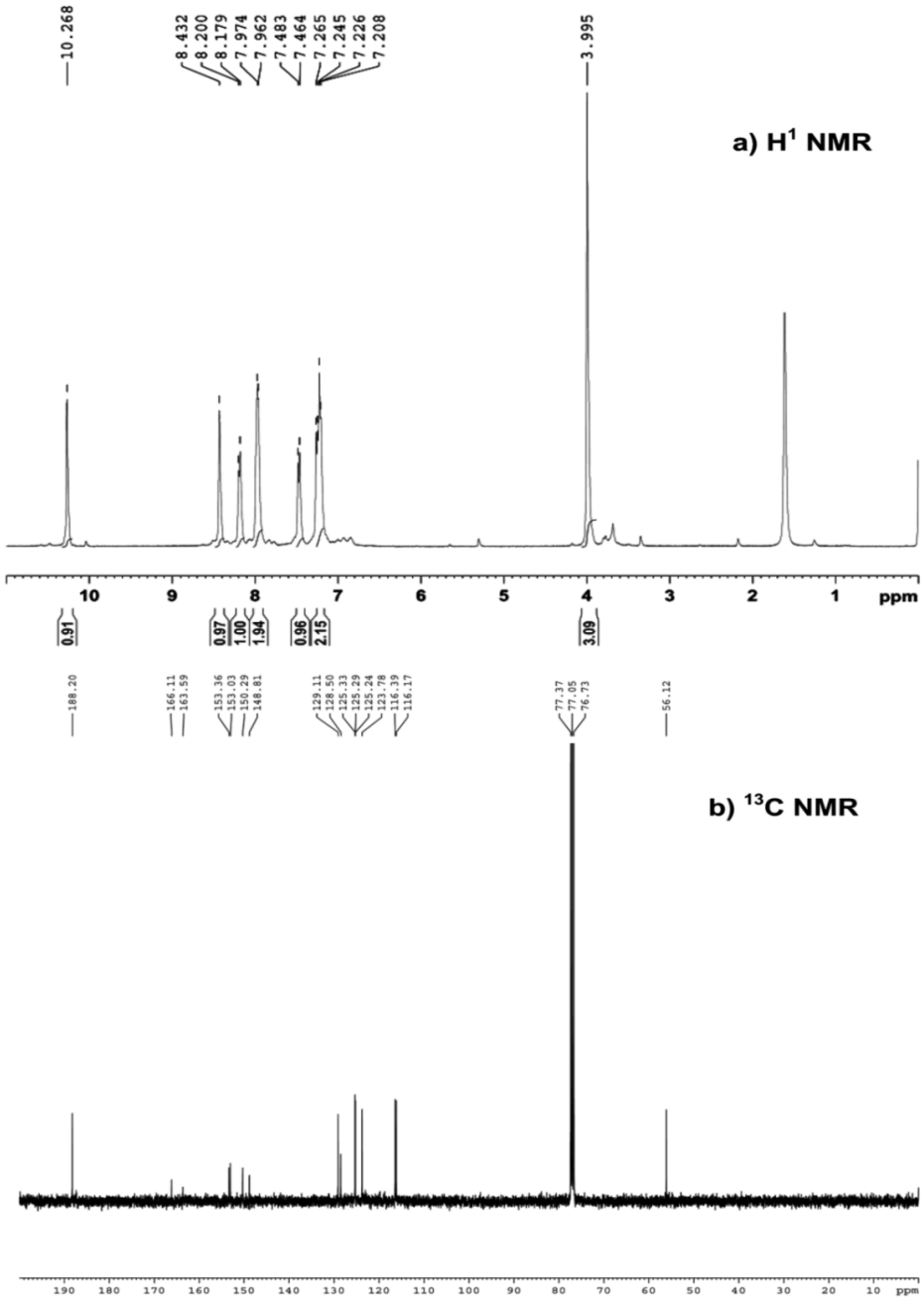

Figure 7. (a) ^{1}H and (b) ^{13}C NMR spectra of FFPMC in $CDCl_3$

The deshielded signals for carbonyl carbon of aldehyde (C30) and carbonate carbon (C23) appeared at 188.2 and 166.11 ppm, respectively. The signal at 153.4, 153.0 and 148.8 ppm are assigned to C20, C13 and C4 which are more deshielded than other ring carbons due to N11–N12 and O22–C23–O24–O25 bonds. The RMS values for carbon chemical shifts were found to be 0.987 and standard deviation was 4.929 for B3LYP method using 6–31+G (d, p) basis set.

Table 6. Experimental and theoretical ^{1}H and ^{13}C chemical shift (ppm) values of FFPMC

Atom	HF	B3LYP	Expt.	Atom	HF	B3LYP	Expt.
H7	6.571	7.883	7.245	C1	162.29	166.1	166.1
H8	7.786	8.872	7.974	C2	114.57	117.1	123.8
H9	7.887	8.768	7.962	C3	119.17	116.6	116.4
H10	6.724	8.032	7.265	C4	144.8	148.8	148.8
H17	8.288	9.053	8.432	C5	187.1	136.6	128.5
H19	8.034	9.050	8.189	C6	114.28	116.1	116.2
H21	6.599	7.853	7.473	C13	145.59	149.7	153.0
H27	1.910	3.745	3.995	C14	141.85	141.4	129.1
H28	2.355	4.304	3.995	C15	124.96	121.4	125.2
H29	2.276	4.109	3.995	C16	126.59	129.3	125.3
H32	8.901	10.776	10.268	C18	121.53	124.8	125.3
				C20	152.65	153.5	153.4
				C23	144.25	149	150.3
				C26	50.917	61.4	56.1
				C30	185.63	188.1	188.2

3.8 Molecular Electrostatic Potential

The MEP is a plot of electrostatic potential computed on electron density; MEP is an effective tool for interpreting and predicting the molecule's reactive behaviour towards electrophiles [41]. The different values of the electrostatic potential at the surface are represented by different colors. Potential increases in the order red < orange < yellow < green < blue. The red region represents most negative electrostatic potential (electrophilic attack), blue region represents most positive electrostatic potential (nucleophilic attack) and green region represents zero potential.

To predict the reactive sites for electrophilic and nucleophilic attack of FFPMC, the MEP have been calculated by B3LYP/6–31+G(d,p) method. This molecule is encompassed by a characteristic three dimensional surface corresponding to contour of 0.002 a.u. isodensity surface. As seen in the Fig. 8 the potential region of the map is in the range between -1.157 to 1.157 (B3LYP) and -0.979 to 0.979 (HF). Furthermore, the reactive sites of compound FFPMC is in favour of electrophilic attack. The negative region is mainly localized on the oxygen atom of the carbonate (O24).

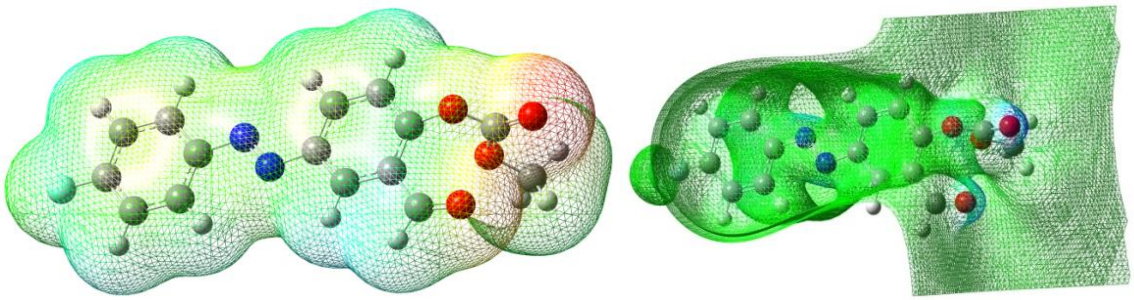

Figure 8. (a) Electron density surface mapped with ESP and (b) ESP mapped with total density of FFPMC

3.9 NLO Properties

The first order hyperpolarizabilities (β_0) and related properties (μ, α_{total}, α_0) of the compound FFPMC have been calculated using HF and B3LYP methods with 6–31+G(d,p) basis set. Molecules having higher values of dipole moment, molecular polarizability and first hyperpolarizability show more active NLO properties [42]. The total dipole moment, mean polarizability, anisotropy of polarizability and mean first order hyperpolarizability, using the x, y, z components are defined as

$$\mu = (\mu_x^2 + \mu_y^2 + \mu_z^2)^{1/2} \quad (1)$$

$$\alpha_0 = (\alpha_{xx} + \alpha_{yy} + \alpha_{zz})/3 \quad (2)$$

$$\alpha_{total} = 2^{-1/2}[(\alpha_{xx} - \alpha_{yy})^2 + (\alpha_{yy} - \alpha_{zz})^2 + (\alpha_{zz} - \alpha_{xx})^2 + 6(\alpha^2_{xx} + \alpha^2_{yy} + \alpha^2_{zz})]^{1/2} \quad (3)$$

$$\beta_x = (\beta_{xxx} + \beta_{xyy} + \beta_{xzz}) \quad (4)$$

$$\beta_y = (\beta_{yyy} + \beta_{xxy} + \beta_{yzz}) \quad (5)$$

$$\beta_z = (\beta_{zzz} + \beta_{xxz} + \beta_{yyz}) \quad (6)$$

$$\beta_0 = (\beta_x^2 + \beta_y^2 + \beta_z^2)^{1/2} \quad (7)$$

The first hyperpolarizability (β) and along with related properties (μ, α_{total} and α_0) are listed in Table 7. The calculated dipole moment equals to 4.90 and 4.73 for HF and B3LYP methods, respectively. The average polarizability (α) is equal to 4.403×10^{-23} e.s.u and 4.168×10^{-23} e.s.u for HF and B3LYP methods, respectively which are almost 1.68 times greater than that of *p*–nitroaniline, a typical NLO material [43–45]. Urea is one of the prototype molecule used in the study of the NLO properties of molecular systems [46]. Therefore, it is used frequently as a threshold value for comparative purposes [47], ($\beta = 0.3728\times10^{-30}$ e.s.u). Furthermore, the total first order hyperpolarizability (β) is equal to.1.37×10^{-30} e.s.u and 1.38×10^{-30} e.s.u of HF and B3LYP method, respectively which is 3.68 times greater than the magnitude of urea.

Besides, efficient second order NLO properties are usually related to compounds that present intramolecular charge transfer (ICT). These ICT processes are usually of one dimensional character, being associated to appreciable dipole moment changes, between the ground and the first excited state, currently identified as the "charge transfer state" related to the electron transfer between these states [48,49]. FFPMC show push-pull type of properties such as para conjugated molecules with a D-p-A structure that exhibit push-pull properties, where D and A are electron donor and acceptor groups, respectively.

This push-pull characteristic generally leads to high or less β value which can be further changes to an adequate substitution of D and A groups. The parameters δ_D and δ_A are used to characterize the effectiveness of donor and acceptor groups. Here, δ_D stands for the energy difference between the

calculated HOMO of the donor-substituted HPDB (2-hydroxy-5-(phenyldiazenyl)benzaldehyde) as a model compound [27] and δ_A stands for the energy difference between the calculated LUMO of the acceptor-substituted HPDB as a model compound and that of HPDB ie $\delta_A=E(LUMO)_A-E(LUMO)_P$ where $E(LUMO)_A$ the represents lowest unoccupied orbital energy of the A acceptor substituted HPDB. The strength of donor-acceptor pairs is characterized by $\delta_{DA} = \delta_D - \delta_A$. From our calculated results, we find that the δ_{DA} value of FFPMC is 0.164 eV. From the literature [47], around the interval of δ_{DA} is 1.2 to 1.5 eV almost in the quinoid form possessing weak enhanced first-order (β) and second-order (γ) NLO susceptibilities. Therefore, FFPMC possess weak enhanced first-order (β) and second-order (γ) NLO susceptibilities.

Table 7. Calculated dipole moment (μD), polarizability (α_0) and first hyperpolarizability (β_{total}) of FFPMC

Parameters	HF	B3LYP	Parameters	HF	B3LYP
Polarizability			Hyperpolarizability		
α_{xx}	-168.99	-160.56	β_{xxx}	-98.97	-101.03
α_{yy}	-113.08	-114.72	β_{xxy}	-29.88	-21.88
α_{zz}	-124.92	-123.97	β_{xyy}	-31.57	-31.61
α_0	-135.66	-133.09	β_{yyy}	-2.24	-4.51
α_{total}	4.403×10^{-23}	4.168×10^{-23}	β_{xxz}	103.87	103.71
$*\alpha_{total}$	3.51×10^{-23}	3.33×10^{-23}	β_{xyz}	-6.87	-0.35
$*\alpha_{total}$	4.74×10^{-23}	4.45×10^{-23}	β_{yyz}	0.47	1.91
Dipole moment			β_{xzz}	43.44	39.52
μ_x	-4.16	-3.97	β_{yzz}	2.44	3.93
μ_y	-0.31	-0.33	β_{zzz}	24.42	21.47
μ_z	2.57	2.57	β_{total}	1.37×10^{-30}	1.38×10^{-30}
μ	4.9	4.73	$*\beta_{total}$	2.17×10^{-30}	2.15×10^{-30}
*μ	6.63	6.32	$*\beta_{total}$	1.45×10^{-30}	1.51×10^{-30}
*μ	4.56	4.55			

*Ref [50]

3.10 Thermodynamic properties

The total energy of a molecule is the sum of translational, rotational, vibrational and electronic energies. The temperature dependence of thermodynamic properties of heat capacity at constant pressure (Cp), entropy (S) and zero–point vibrational energy were determined by HF and B3LYP levels with 6–31+G(d,p) basis set and the values are listed in Table 8.

Table 8 Calculated thermodynamic parameters of FFPMC

Parameters	HF	B3LYP
SCF energy (a.u.)	-1082.23	-1088.47
Total energies (kcal/mol)	172.65	161.56
Zero point energy (kcal/mol)	161.27	149.46
Rotational constants (GHz)		
x	1.03	1.03
y	0.09	0.09
z	0.08	0.08
Entropy (cal/mol-K)	144.09	148.56
Heat capacity (cal/mol-K)	66.39	71.36

This statistical thermochemical analysis was carried out at room temperature 298.15 K at 1 atm. pressure. From the results of Table 8, FFPMC has minimum total energy (-1088.47 a.u) by B3LYP compared with HF method (-1082.23 a.u). The scale factors [29] have been used for accurate determination of thermodynamic properties.

4. CONCLUSION

FFPMC was synthesized and characterized by various spectroscopic methods. A complete vibrational assignments were determined and analyzed on the basis of TED by HF and B3LYP functional with 6–31+G(d,p) basis set which are found in good agreement with the experimental values. The dipole moment, polarizability and hyperpolarizability data indicate that the FFPMC possess push-pull behavior. Besides, the difference in HOMO and LUMO energies supports the charge transfer interactions present within the molecule. Furthermore, the NBO analysis and thermodynamic parameters confirmed the ability of the methodology applied for the interpretation of the vibrational spectra of the title compound in the solid phase.

REFERENCES

[1] Catino, S. C.; Farris, E. *Concise Encyclopedia of Chemical Technology*, John Wiley & Sons: New York, 1985.

[2] Venkataraman, K.; *The Chemistry of Synthetic Dyes*, Academic Press, New York and London, 1970 (Chapter VI).

[3] Egli, R.; Peter, A. P. *Colour chemistry: the Design and Synthesis of Organic Dyes and Pigments*, Freeman H. S. Ed.; Elsevier: London, 1991 (Chapter VII).

[4] Emeleus, L. C.; Cupertino, D. C. Harris, S. G. Owens, S. Parsons, S. Swart, R. W. Tasker, P. A. White, D. J. Diazopyrazolones as Weak Solvent Extractants for Copper From Ammonia Leach Solutions. *Dalton Trans*. **2001**, 1239–1245.

[5] Rau, H.; *Photochemistry and Photophysics*, CRC Press, Boca Raton: Florida, 1990; vol. 2; p119–141.

[6] Balaraman, E. Gunanathan, C. Zhang, J. Shimon, L. Milstein, J. W. D. Efficient Hydrogenation of Organic Carbonates, Carbamates and Formates Indicates Alternative Routes to Methanol Based on CO_2 and CO. *Nature Chemistry*. **2011**, *3*, 609–614.

[7] Olie, G.; Olive, S. *The Chemistry of the Catalyzes Hydrogenation of Carbon Monoxide*, Springer: Berlin, 1984.

[8] Parrish, J. P.; Salvatore, R. N. Jung, K. W. Perspectives on Alkyl Carbonates in Organic Synthesis. *Tetrahedron* **2000**, *56*, 8207–8237.

[9] Sakakura, T.; Kohno, K. The Synthesis of Organic Carbonates from Carbon Dioxide. *Chem. Commun*. **2009**, 1312–1330.

[10] Schaffner, B.; Schaffner, F. Verevkin, S. P. Borner, A. Organic Carbonates as Solvents in Synthesis and Catalysis. *Chem. Rev.* **2010**, *110*, 4554 –4581.

[11] Zhang, H.; Liu, H. B. Yue, J. M. Organic Carbonates from Natural Sources. *Chem. Rev*. **2014**, *114*, 883−898.

[12] Arteconi, A.; Mazzarini, A. Nicola G. D. Emissions from Ethers and Organic Carbonate Fuel Additives: A Review. *Water Air Soil Pollut*. **2011**, *221*, 405–423.

[13] Kim, S.; Chu, F. Dueno, E. E. Jung, K. W. Alkyl Carbonates: Efficient Three Component Coupling of Aliphatic Alcohols, CO_2, and Alkyl Halides in the Presence of Cs_2CO_3. *J. Org. Chem.***1999**, *64*, 4578–4579.

[14] Grynkiewicz, G.; Jurczak, J. Zamojski, A. The Synthesis of Mixed Carbonates From Alcohols, Dialkyl Azodicarbozylate and Tris(dimethylamino)-phosphine. *Tetrahedron* **1975**, *31*, 1411–1414.

[15] Burk, R. M.; Roof, M. B. A safe and Efficient Method for Conversion of 1,2- and 1,3-Diols to Cyclic Carbonates Utilizing Triphosgene. *Tetrahedron Lett*. **1993**, *34*, 395–398.

[16] Shaikh, A. A. G.; Sivaram, S. Organic Carbonates. *Chem. Rev*. **1996**, *96*, 951–976.

[17] Yadav, J. S.; Sudershan Reddy, G. Muralidhar Reddy, M. Meshram, E. I. M. Zinc Promoted Simple and Convenient Synthesis of Carbamates : An Easy Access for Amino Group Protection. *Tetrahedron Lett.* **1998**, *39*, 3259–3262.

[18] Mormeneo, D.; Llebaria, A. Delgado, A. A practical Synthesis of Carbamates Using an In-Situ Generated Polymer-Supported Chloroformate. *Tetrahedron Lett*. **2004**, *45*, 6831–6864.

[19] Sivakumar, R.; Gokula Krishnan, K. Thanikachalam, V. Bioorganic Synthesis, Spectral and Antimicrobial Evaluation of Some Novel 1-methyl-3-alkyl-2,6-diphenylpiperidin-4-one Oxime Carbonates. Bio org. *Med. Chem. Lett*. **2013**, *23*, 3195–3199.

[20] Odabasoglu, M.; Albayrak, C. Ozkanca, R. Aykan, F. Z. Lonecke, P. Some Polyhydroxy Azo–Azomethine Derivatives of Salicylaldehyde: Synthesis, Characterization, Spectroscopic, Molecular Structure and Antimicrobial Activity Studies. *J. Mol. Struct.* **2007**, *840*, 71–89.

[21] Montgomery, J. A.; Vreven, T. Kudin, K. N. Burant, J. C. Millam, J. M. Iyengar, S. S. Tomasi, J. Barone, V. Mennucci, B. Cossi, M. Scalmani, G. Rega, N. Petersson, G. A. Nakatsuji, H. Hada, M. Ehara, M. Toyota, K. Fukuda, R. Hasegawa, J. Ishida, M. Nakajima, T. Honda, Y. Kitao, O. Nakai, H. Klene, M. Li, X. Knox, J. E. Hratchian, H. P Cross, J. B. Bakken, V. Adamo, C. Jaramillo, J. Gomperts, R. Stratmann, R. E. Yazyev, O. Austin, A. J. Cammi, R. Pomelli, C. Ochterski, J. W. Ayala, P. Y. Morokuma, K. Voth, G. A. Salvador, P. Dannenberg, J. J. Zakrzewski, V. G. Dapprich, S. Daniels, A. D. Strain, M. C. Farkas, O. Malick, D. K. Rabuck, A. D. Raghavachari, K. Foresman, J. B. Ortiz, J. V. Cui, Q. Baboul, A. G. Clifford, S. Cioslowski, J. Stefanov, B. B. Liu, G. Liashenko, A. Piskorz, P. Komaromi, I. Martin, R. L. Fox, D. J. Keith, T. Al–Laham, M. A. Peng, C. Y. Nanayakkara, A. Challacombe, M. Gill, P. M. W. Johnson, B. Chen, W. Wong, M. W. Gonzalez, C. Pople, J. A. *Gaussian 03 Revision C.02*. Gaussian Inc., Wallingford CT, 2004.

[22] Lee, C.; Yang, W. Parr, R. G. Development of the Colic-Salvetti Correlation-Energy Formula into a Functional of the Electron Density. *Phys. Rev. B.* **1988**, *37*, 785–789.

[23] Becke, A. D.; Density Functional Thermochemistry. III. The Role of Exact Exchange. *J. Chem. Phys.***1993**, *98*, 5648–5652.

[24] Frish, A.; Nielson, A. B. Holder, A. J. *Gaussview User Manual*. Gaussian Inc., Pittsburg, pA, 2000.

[25] Albayrak, C.; Gumrukcuoglu, I. E. Odabasoglu, M. Buyukgungor, O. (E)-2-Methyl-4-(phenyldiazenyl)phenol. *Acta Cryst. E.* **2007**, *63*, 3662–3663.

[26] Palafox, M. A.; Scaling Factors for the Prediction of Vibrational Spectra. II. The Aniline Molecule and Several Derivatives. *Int. J. Quantum Chem*. **2000**, *77*, 661–684.

[27] Bharanidharan, S.; Saleem, H. Nathiya, A. Arokiasamy, A. Thanikachalam, V. Spectroscopic Investigations of (*E*)-5-(2-phenyldiazenyl)-2-hydroxybenzaldehyde Using DFT Method. *Int. Lett. Chem. Phys. Astron.* **2015**, *60*, 168-181.

[28] Palafox, M. A.; Gill, M. Nunez, N. J. Rastogi, V. K. Mittal, L. Sharma, R. Scaling Factors for the Prediction of Vibrational Spectra. II. The Aniline Molecule and Several Derivatives. *Int. J. Quantum Chem*. **2005**, *103*, 394–421.

[29] Stuart, B.H.; *Infrared spectroscopy: Fundamentals and Applications.* John Wiley & Sons: Chichester, U.K, 2004.

[30] Uno, T.; Lee, H.; Saito, Y. Resonance Raman Spectra of p-hydroxyazobenzene and its Ring-Deuterded derivatives. *Spectrochim. Acta*. **1976**, *32*, 1319–1322.

[31] Muthu, S.; Ramachandran, G. Umamaheswari, J. Vibrational Spectroscopic Investigation on the Structure of 2-ethylpyridine-4-carbothioamide. *Spectrochim. Acta Part A Mol. Biomol. Spectrosc*. **2012**, *93*, 214–222.

[32] Mulliken, R. S.; Electronic Population Analysis on Lcaomo Molecular Wave Functions I. *J. Chem. Phys*. **1955**, *23*, 1833–1840.

[33] Mulliken, R. S.; Electronic Population Analysis on Lcaomo Molecular Wave Functions. II. Overlap Populations, Bond Orders, and Covalent Bond Energies. *J. Chem. Phys*. **1955**, *23*, 1841–1846.

[34] Cramer, C. J.; *Essentials of Computational Chemistry: Theories and Models*, 2nd Ed., Wiley; Hoboken, NJ, 2004.

[35] Snehalatha, M.; Ravikumar, C. Hubert Joe, I. Sekar, N. Jayakumar, V. S. Spectroscopic Analysis and DFT Calculations of a Food Additive Carmoisine. *Spectrochim Acta Part A Mol Biomol. Spectrosc*. **2009**, *72*, 654–662.

[36] Fleming, I.; *Frontier Orbitals and Organic Chemical Reactions*. Wiley–Blackwell: New York, 1976.

[37] Koopmans, T.C.; By Assigning Wave Functions and Eigen Values for the Individual Electrons of an Atom. *Physica. (Amsterdam*) **1993**, *1*, 104–113.

[38] Ebrahimi, H. P.; Shaghaghi, H. Tafazzoli, M. Gauge Invariant Atomic Orbital-Density Functional Theory Prediction of Accurate Gas Phase ^{1}H and ^{13}C NMR Chemical Shifts. *Concepts in Magnetic Resonance Part A.* **2011**, *38*, 269–279.

[39] Pavia, D. L.; Lampman, G. M. Kriz, G. S. Vyvyan, J. R. *Introduction to Spectroscopy*, 4th Ed., Brooks/Cole, Belmont; USA, 2009.

[40] Manimekalai, A.; Balachander, R. Theoretical Investigation of the Conformation and Hydrogen Bonding Ability of 5-arylazosalicylaldoximes. *J. Mol. Struct.* **2012**, *1027*, 175–185.

[41] Murray, J. S.; Sen, K. *Molecular Electrostatic Potentials, Concepts and Applications.* Elsevier: Amsterdam, 1996.

[42] Nakano, M.; Shigemoto, I. Yamada, S. Yamaguchi, K. Theoretical Study on Second Hyperpolarizabilities of Phenylacetylene Dendrimer: Toward an Understanding of Structure-Property Relation in NLO Responses of Fractal Antenna Dendrimers. *J. Chem. Phys.* **1995**, 103, 4175– 4191.

[43] Cheng, L. T.; Tam, W. Stevenson, S. H. Meredith, G. R. Riklen, G. R. Marder, S. Experimental Investigations of Organic Molecular Nonlinear Optical Polarizabilities. 1. Methods and Results on Benzene and Stilbene Derivatives. *J. Phys. Chem*. **1991**, *95*, 10631–10643.

[44] Kaatz, P.; Donley, E. A. Sheton, D. P. A Comparison of Molecular Hyperpolarizabilities From Gas and Liquid Phase Measurements. *J. Phys. Chem.* **1998**, *108*, 849–856.

[45] Gerrat, J.; Mills, I. M. Force Constants and Dipole Moment Derivatives of Molecules from Perturbed Hartree–Fock Calculations. *J. Chem. Phys.* **1968**, *49*, 1719–1729.

[46] Pulay, P.; Second and Third Derivatives of Vibrational Energy Expressions: Application to Multiconfigurational Self Consistent Field Wave Functions. *J. Chem. Phys*. **1983**, 78, 5043–5051.

[47] Wu, K.; Snijders, J. G. Lin, C. Reinvestigation of Hydrogen Bond Effects on the Polarizability and Hyperpolarizability of Urea Molecular Clusters. *J. Phys. Chem. B.* **2002**, *106*, 8954–8958.
[48] Kanis, D. R.; Ratner, M. A. Marks, T. J. Design and Construction of Molecular Assemblies with Large Second-Order Optical Nonlinearities Quantum Chemical Aspects. *Chem. Rev.* **1994**, *94*, 195–242.
[49] Oudar, J. L.; Optical Nonlinearities of Conjugated Molecules Stilbene Derivatives and Highly Polar Aromatic Compounds. *J. Chem. Phys.* **1977**, *67*, 446–457.
[50] Arokiasamy A.; Manikandan, G. Thanikachalam, V. Gokula Krishnan, K. Synthesis, Spectroscopic Investigation and Computational Studies of 2-formyl-4-(phenyldiazenyl)phenyl Methyl Carbonate and 4-((4-chlorophenyl)diazenyl)-2-formylphenyl Methyl Carbonate. *Int. Lett. Chem. Phys. Astron.* **2016**, *66*, 38–70.

The authors declare no conflict of interest

© 2016 By the Authors; Licensee Borderless Science Publishing, Canada. This is an open access article distributed under the terms and conditions of the Creative Commons Attribution license http://creativecommons.org/licenses/by/3.0